












The ALMA REBELS Survey: the first infrared luminosity function measurement at $z \sim 7$

L. Barrufet ^{1,★}, P. A. Oesch ^{1,2}, R. Bouwens,³ H. Inami ⁴, L. Sommovigo ⁵, H. Algera ^{4,6},
E. da Cunha,⁷ M. Aravena,⁸ P. Dayal ⁹, A. Ferrara,⁵ Y. Fudamoto,^{6,10} V. Gonzalez,^{11,12} L. Graziani ^{13,14},
A. P. S. Hygate ³, I. de Looze,^{15,16} T. Nanayakkara,¹⁷ A. Pallottini ⁵, R. Schneider ^{13,14},
M. Stefanon,^{18,19} M. Topping ²⁰ and P. van der Werf³

Affiliations are listed at the end of the paper

Accepted 2023 March 30. Received 2023 March 20; in original form 2022 September 30

ABSTRACT

We present the first observational infrared luminosity function (IRLF) measurement in the Epoch of Reionization (EoR) based on a ultraviolet (UV)-selected galaxy sample with the Atacama Large Millimeter Array (ALMA) spectroscopic observations. Our analysis is based on the ALMA large program Reionization Era Bright Emission Line Survey (REBELS), which targets 42 galaxies at $z = 6.4\text{--}7.7$ with [C II] 158 μm line scans. 16 sources exhibit dust detection, 15 of which are also spectroscopically confirmed through the [C II] line. The infrared (IR) luminosities of the sample range from $\log L_{\text{IR}}/L_{\odot} = 11.4$ to 12.2. Using the UV luminosity function as a proxy to derive the effective volume for each of our target sources, we derive IRLF estimates, both for detections and for the full sample including IR luminosity upper limits. The resulting IRLFs are well reproduced by a Schechter function with the characteristic luminosity of $\log L_{*}/L_{\odot} = 11.6^{+0.2}_{-0.1}$. Our observational results are in broad agreement with the average of predicted IRLFs from simulations at $z \sim 7$. Conversely, our IRLFs lie significantly below lower redshift estimates, suggesting a rapid evolution from $z \sim 4$ to $z \sim 7$, into the reionization epoch. The IR obscured contribution to the cosmic star formation rate density at $z \sim 7$ amounts to $\log(\text{SFRD}/M_{\odot} \text{ yr}^{-1} \text{ Mpc}^{-3}) = -2.66^{+0.17}_{-0.14}$ that is at least ~ 10 per cent of UV-based estimates. We conclude that the presence of dust is already abundant in the EoR and discuss the possibility of unveiling larger samples of dusty galaxies with future ALMA and *JWST* observations.

Key words: galaxies: high-redshift – galaxies: luminosity function, mass function – infrared: galaxies.

1 INTRODUCTION

It is still a crucial open question in astrophysics when the first galaxies formed and how they built up their mass. The continuous discovery of higher redshift galaxies is pushing the boundaries of our knowledge of galaxy evolution (e.g. Dunlop 2013; Stark 2016; Dayal & Ferrara 2018; Naidu et al. 2022a; Schaerer et al. 2022; Adams et al. 2023; Atek et al. 2023). In particular, the discovery of a significant population of luminous and massive galaxies at $z > 9$ has posed questions about the speed of early stellar mass production (e.g. Oesch et al. 2016; Laporte et al. 2021; Naidu et al. 2022b; Labbe et al. 2023).

Until recently, the knowledge of galaxies at $z > 7$ was mainly based on rest-frame ultraviolet (UV) observations (Oesch et al. 2018a; Bouwens et al. 2022a). These samples might not be complete, however, as they might miss extremely dust obscured, but highly star-forming galaxies (e.g. Casey et al. 2019).

From an observational point of view, the Atacama Large Millimeter Array (ALMA) is the most powerful tool to study dust at high redshift (e.g. Capak et al. 2015; Bouwens 2016; Bowler et al. 2018; Béthermin et al. 2020). However, the cost to obtain statistical

samples of galaxies in the Epoch of Reionization (EoR) results in the fact that only a modest number of galaxies have been characterized in detail so far (e.g. Watson et al. 2015; Smit et al. 2018; Laporte et al. 2019; Faisst et al. 2020; Harikane et al. 2022; Schouws et al. 2022b). Furthermore, the study of dust at $2 < z < 6$ was for a long time limited to bright dusty galaxies such as submillimetre galaxies (SMGs; e.g. Gruppioni et al. 2013; Wang et al. 2019b; Barrufet et al. 2020). However, ALMA is bridging the gap between these extremely dusty massive galaxies and more moderate star-forming galaxies (see Hodge & da Cunha 2020 for a review).

The recent observational improvements have allowed the discovery of the emergence of high- z dusty galaxies at $z > 6$. In particular, Fudamoto et al. (2021) have serendipitously detected two dusty galaxies at $z_{\text{spec}} \sim 7$ near massive neighbours at the same redshifts. This shows that dusty galaxies in the EoR could be more common than previously thought, which leads to the question of whether the number of dusty galaxies at $z > 6$ is higher than expected (see also Nelson et al. 2022; Barrufet et al. 2023; Rodighiero et al. 2023).

The possible underestimation of the number of dusty galaxies would have a direct impact on the obscured star formation rate density (SFRD), which remains uncertain at $z > 3$ (Casey et al. 2019). Several studies have calculated the obscured SFRD at $z > 5$ based on serendipitous sources resulting in largely differing conclusions (e.g. Gruppioni et al. 2020; Casey et al. 2021; Fudamoto

* E-mail: laia.barrufetdesoto@unige.ch

et al. 2021; Talia et al. 2021; Viero et al. 2022). While some studies find that 2-mm selected dusty galaxies contribute ~ 30 per cent to the integrated SFRD in the range $3 < z < 6$ (Casey et al. 2021), others report a significantly larger obscured SFRD that remains constant over redshift (e.g. Gruppioni et al. 2020; Talia et al. 2021). An approach to clarify the contribution of dust-obscured star formation to the cosmic star formation history is to measure the infrared luminosity function (IRLF) all the way into the EoR. The shape and scale of the IRLF are crucial to understanding the abundance of dusty galaxies and how rapidly dust is formed in the early Universe. This directly affects the fraction of star formation that is obscured in forming galaxies, and thereby the formation (or rise) of metals.

Because of the wealth of rest-frame UV observations, the UV luminosity function (UVLF) is well constrained up to $z \sim 9$ (e.g. Bouwens et al. 2007, 2015, 2021; Oesch et al. 2018b; Bowler et al. 2020), and we even have some information at $z \sim 9$ –10 (Oesch et al. 2018a; Harikane et al. 2023) and beyond now with *JWST* (e.g. Finkelstein et al. 2022; Naidu et al. 2022b; Adams et al. 2023; Atek et al. 2023; Donnan et al. 2023). In contrast, the IRLF is still quite uncertain at high redshifts. Current measurements of the IRLF rely on small numbers of dusty sources at $z > 3.5$ (e.g. Wang et al. 2019a; Gruppioni et al. 2020). This leads to large uncertainties in the IRLF parameters, including the faint-end slopes, and disagreements between different survey results (e.g. Gruppioni et al. 2013, 2020; Koprowski et al. 2017; Lim et al. 2020; Popping et al. 2020).

The recent study of Zavala et al. (2021) compiled the results of several surveys and combined those with semi-empirical modelling to constrain the evolution of the IRLF out to $z > 5$, albeit with significant uncertainties. However, an IRLF at $z \sim 7$ has not been measured directly using dust continuum observations yet. In this context, we use the data from the Reionization Era Bright Emission Line Survey (REBELS), an ALMA large program aimed at obtaining a statistical sample of normal star-forming galaxies at $z > 6.4$ (see Bouwens et al. 2022b for details). REBELS has increased the number of spectroscopically observed massive galaxies in the EoR by a factor of ~ 4 –5 compared to the previous literature (Bouwens et al. 2022a). The same strategy of the REBELS selection was tested in a pilot program presented in Schouws et al. (2022b). This study showed the potential of ALMA as a high-redshift ‘machine’ and the six pilot galaxies are also included in the main REBELS sample (Smit et al. 2018; Schouws et al. 2022a,b). While observations from the REBELS program were just recently completed and analysis of the full data set is now underway, its data have already been used for a number of scientific analyses, including the discovery of serendipitous dust-obscured sources at $z \sim 7$ (Fudamoto et al. 2021), modelling the dust and interstellar medium (ISM) properties of $z > 6$ galaxies (e.g. Dayal et al. 2022; Ferrara et al. 2022; Sommovigo et al. 2022a), measuring their detailed specific star formation rates (SFRs; Topping et al. 2022), calculating their SFRD (Algera et al. 2023), estimating Ly α transmission around luminous sources in overdense $z \sim 7$ environments (Endsley et al. 2022), and constraining the neutral gas fraction out to the EoR (Heintz et al. 2022).

In this paper, we use this survey to calculate – for the first time – an IRLF at $z \sim 7$. In Section 2, we describe the ALMA observations and the infrared (IR) luminosity calculations used in this work. The methodology for calculating the IRLF and their values is described in Section 3. We present the results on the obscured SFRD of REBELS galaxies in Section 4. We discuss our results in Section 5 and present a summary and our conclusions in Section 6.

2 REBELS OBSERVATIONS

2.1 ALMA observations and catalogue

In this work, we use data from REBELS (Bouwens et al. 2022a) that is a Cycle 7 ALMA large program of ~ 40 UV-bright galaxies at $z > 6.4$. The selection was based on UV brightness ($-23 < M_{UV} < -21.3$) and photometric redshifts for galaxies identified over a combined area of ~ 7 deg² in several fields (see Bouwens et al. 2022a for details). This survey of spectral scan observations identifies bright ISM cooling lines ([C II], [O III]) while simultaneously probing the dust continuum in bands 158 and 88 μm , respectively, which is essential to derive the IR luminosity (L_{IR}). Given its selection, the REBELS sample only spans a limited range in redshift and UV luminosities. Even though it is UV selected, the sample is representative of massive star-forming galaxies at $z \sim 7$, providing an extensive probe of ISM reservoirs in the EoR (Bouwens et al. 2022b; Ferrara et al. 2022).

In this work, we only focus on galaxies that were scanned for [C II], i.e. sources with $z_{\text{phot}} = 6.4$ –7.7. The total sample used in this study contains 42 galaxies with [C II] scanned, 16 of which with a dust continuum detection at more than 3σ . Notably, 15 of these 16 sources also do have a significant [C II] emission line detection and thus a robust spectroscopic redshift measurement (Inami et al. 2022).

2.2 Infrared luminosity from REBELS survey

In this section, we describe the IR luminosity measurements from Inami et al. (2022) and the average properties of the REBELS galaxies.

When deriving the IR luminosities of our sample, we have to make an assumption about the dust temperature. Estimating this based on a few photometric detections in the far-IR is very challenging. Sommovigo et al. (2021) solve this difficulty using $L_{[C II]}$ as a proxy for the dust mass and the underlying continuum to constrain the dust temperature. This is particularly useful for the REBELS survey, given that [C II] estimates (or upper limits) are available for the full sample. Using these measurements, Sommovigo et al. (2022a) find an average dust temperature of $T_d = 46$ K for the REBELS sample. Hence, Inami et al. (2022) assumed a spectral energy distribution (SED) with dust temperature and emissivity from Sommovigo et al. (2022a) ($T_d = 46$ K and $\beta = 2$, respectively) to calculate the IR luminosity based on the ALMA dust continuum flux. For the galaxies without dust continuum detection a 3σ upper limit was derived both for the continuum flux and the corresponding IR luminosity. A cosmic microwave background correction was applied for all galaxies, with and without dust detection. The correction depends on the exact redshift but lies in the range of 8–14 per cent (see Inami et al. 2022 for details).

Using the derived IR luminosity measurements, we plot in Fig. 1 the relation between UV and IR luminosities. Given the selection of UV luminous sources, the dynamic range both in UV and IR luminosities is limited. The REBELS sample only probes the most massive, UV luminous galaxies at these redshifts. It is composed of luminous infrared galaxies (LIRGs; $10^{11} < L_{IR}/L_{\odot} < 10^{12}$) except for REBELS-25, the brightest galaxy in our sample with $\log(L_{IR}) \sim 12.2 L_{\odot}$ (see Hygate et al. 2022 for details). The fact that we found only one ultraluminous infrared galaxy (ULIRG; $L_{IR} > 10^{12} L_{\odot}$) in the REBELS sample could be due to the UV bright selection of REBELS galaxies with $-23 < M_{UV} < -21.3$. We discuss this further in a later section.

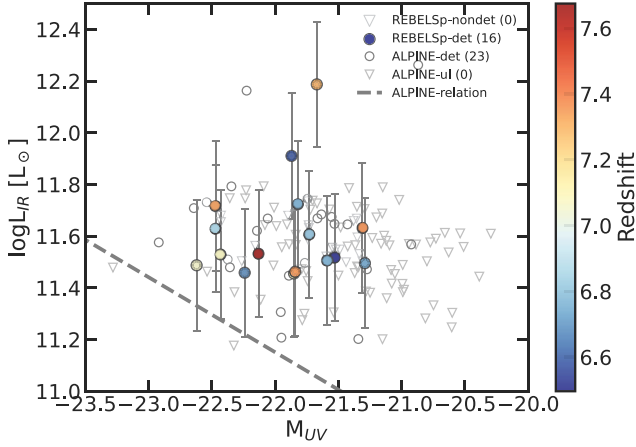


Figure 1. IR luminosity against UV absolute magnitude with the redshift colour coded for the REBELS (filled symbols) and ALPINE (empty symbols) samples for both 3σ detections (dots) and upper limits (triangles). The REBELS sample does not show significant differences between detections and upper limits. L_{IR} does not depend on M_{UV} or redshift. The small L_{IR} dynamic range and the flatness are comparable with the ALPINE sample at $4.5 < z < 6$ although ALPINE extends to fainter UV galaxies (empty triangles and dots for upper limits and detections, respectively). The ALPINE relation presented in Khusanova et al. (2021) is shown in the black dashed line.

We compare the IR luminosities from REBELS with the sample from the ALMA Large Program to INvestigate [C II] at Early times (ALPINE; Le Fèvre et al. 2020) that targets UV-selected sources at lower redshifts at $4.5 < z < 6$. The ALPINE sample spans a wider M_{UV} range ($-23.3 < M_{\text{UV}} < -20$) but is also mostly composed of LIRGs (see Fig. 1) finding also in general dusty galaxies (Pozzi et al. 2021; Sommovigo et al. 2022b). Our REBELS sample shows that UV-selected galaxies at $z \sim 7$ have comparable IR luminosities to UV-selected galaxies at lower redshift ($4.5 < z < 6$) (see Section 5 for discussion).

3 INFRARED LUMINOSITY FUNCTION AT $z \sim 7$

In this section, we explain the procedure to calculate the luminosity function (LF). The main complication in computing a LF using a targeted survey such as REBELS is that it is not straightforward to derive a selection volume for each source. This can be overcome by basing our volume estimates on the UVLF as a proxy, as was successfully demonstrated in Yan et al. (2020) who used the ALPINE UV-targeted sample to derive the [C II] LF. Here, we closely follow their approach.

3.1 Calculation of the luminosity function

Our derivation is based on the $z \sim 7$ UVLF from Bouwens et al. (2022a). This is used to derive a representative volume for the UV-selected sources. In practice, we use the UVLF to compute the number of expected galaxies in bins of UV luminosity assuming a volume-limited survey over the full selection area of the REBELS sample of 7 deg^2 and $z = 6.4\text{--}7.7$ (see Fig. 2). This is given by

$$N_{\text{exp}} = \phi_{\text{UV}}(M_{\text{UV}}) \Delta M_{\text{UV}} V_{\text{tot}}, \quad (1)$$

where $\phi_{\text{UV}}(M)$ is the UVLF from Bouwens et al. (2022a) per magnitude bin ΔM_{UV} , and V_{tot} is the total survey volume over which REBELS sources were selected. REBELS only targets a very small subsample of all galaxies expected in such a large survey.

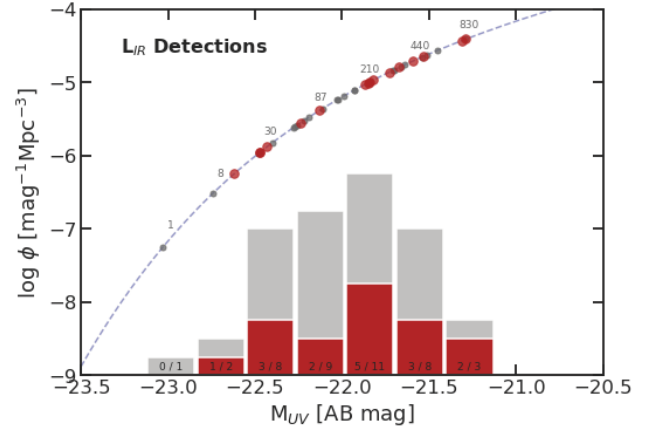


Figure 2. Number of L_{IR} detections against the UV absolute magnitude. The histogram shows the detected sources in red and the non-detections in grey with the fraction of detections/total indicated in the lower numbers. Also shown is the UVLF from Bouwens et al. (2022a) as a dashed line. This is used to compute the representative volume for each of our targets. The small numbers above the LF indicate how many galaxies are expected per M_{UV} bin in a volume-limited survey spanning the REBELS target selection area of 7 deg^2 . Clearly, REBELS only targets a very small fraction of the full galaxy population at faint UV luminosities, which we account for in our analysis (see main text).

We can compute a correction factor to account for this sampling incompleteness in each UV luminosity bin as $f_{\text{UV}} = N_{\text{exp}}/N_{\text{obs}}$, where N_{obs} is the number of targeted REBELS galaxies in each M_{UV} bin.

While the correction factor above is derived for a volume-limited survey, the requirement of a dust continuum detection can further introduce a reduction in the survey volume for each source. Namely, it can limit the maximum redshift up to which a given source would remain detected. This is accounted for by computing the so-called maximum comoving volume $V_{\text{max},i}$ for each galaxy i (see Schmidt 1968). Specifically, $V_{\text{max},i} = \int_{z_{\text{min}}}^{z_{\text{max},i}} d^2V/dz d\Omega dz$, where $z_{\text{max},i}$ is either the upper edge of the redshift bin of the LF, or, if smaller, the maximum redshift up to which source i would remain continuum detected at $>3\sigma$. Ω is the survey volume. In practice, $z_{\text{max},i} = 7.7$ for most galaxies, except for the faintest few sources in the sample.

We now have all quantities to calculate the IR luminosity function ϕ_{IR} in bins of L_{IR} . This is given by

$$\phi_{\text{IR}}(\log L_{\text{IR}}) = \frac{1}{\Delta \log L_{\text{IR}}} \sum_{i \in \text{bin}} \frac{f_{\text{UV},i}}{V_{\text{max},i}}, \quad (2)$$

where i runs over all sources in a given IR luminosity bin $\log L_{\text{IR}} \pm \Delta \log L_{\text{IR}}/2$ (see equation 3 in Yan et al. 2020). The uncertainties on the IRLF bins are computed as the Poisson errors in each L_{IR} bin.

Note that this calculation is independent of the assumed survey area Ω , since both V_{max} and f_{UV} are directly proportional to it.

We repeat the above calculation twice. In the first case, we only consider continuum-detected galaxies (16 sources); in the second case, we include the full REBELS sample (42 sources), treating non-detections as upper limits. The completeness factors f_{UV} are computed separately for both cases. The resulting IRLFs are in very good agreement, as discussed in the next section.

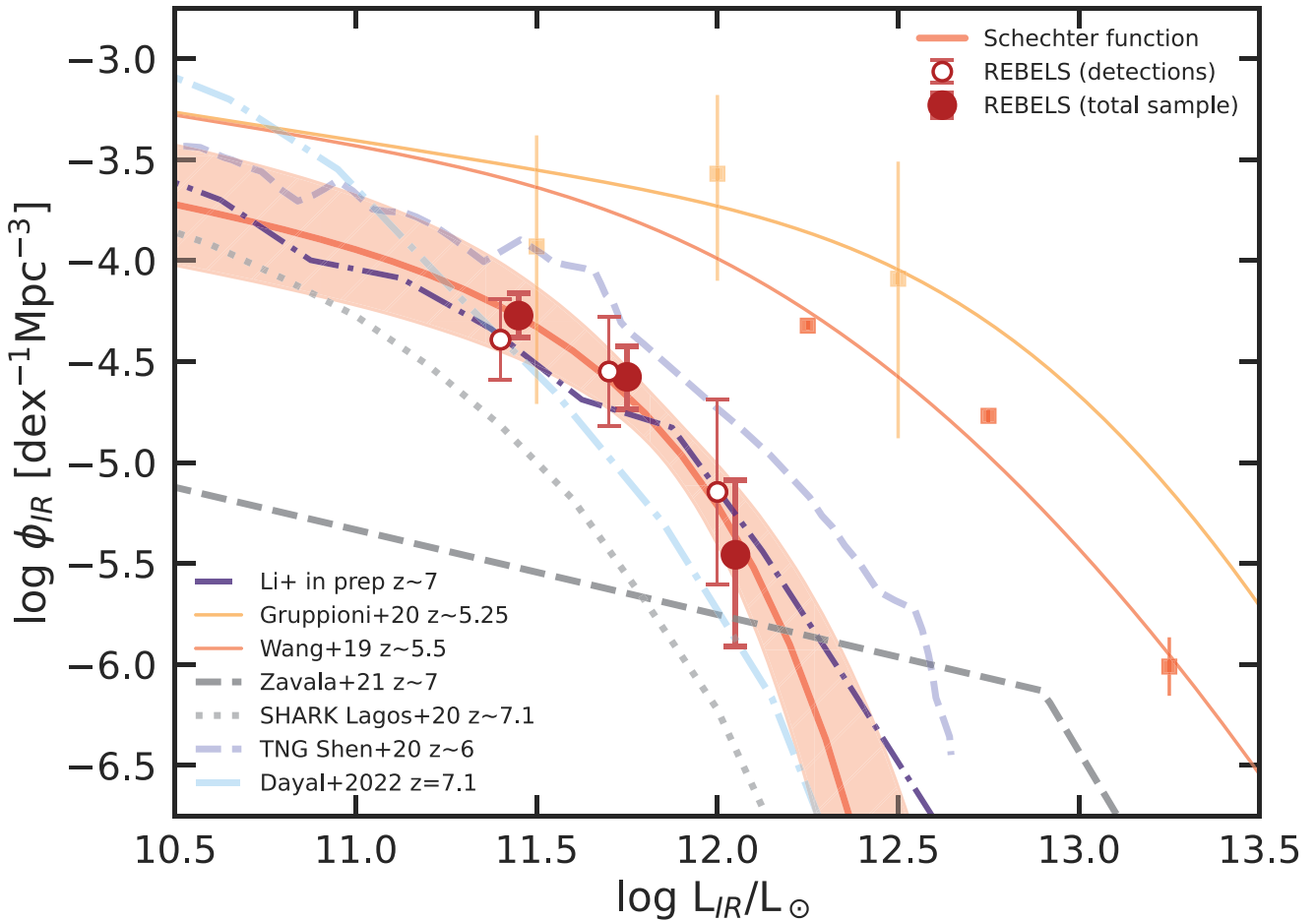


Figure 3. Infrared luminosity function (IRLF) at $z \sim 7$ for the REBELS sample (red dots and lines) compared with simulations (dashed lines) and observations (solid lines). The IRLF was calculated both only using the galaxies with dust continuum detections (16 galaxies, empty dots) and using the full sample including upper limits (42 galaxies, filled red dots). The red line shows the Schechter (1976) fit for the total sample. The shaded area shows the uncertainty of the luminosity function (LF) Schechter function fit with the total sample that is larger at the low-luminosity end due to the lack of data. The rest of the lines show both theoretical and observational IRLF studies in several fields. Our study is in agreement with Li et al. (in preparation, dark purple line) that predict a similar number of dusty galaxies in a broad range of luminosities. The dark grey line is the IRLF at $z \sim 7$ from Zavala et al. (2021) and predicts a larger number of galaxies than our study for the bright end with luminosities ($12.5 < \log(L_{\text{IR}}/L_{\odot}) < 13$), whereas our LF does not predict a significant number of galaxies at $z \sim 7$ with $\log(L_{\text{IR}}/L_{\odot}) > 12.5$). TNG simulations at $z \sim 6$ from Shen et al. (2022) show a systematic shift with respect to our fitting, but consistent in shape (blue dashed line). Dayal et al. (2022) and Lagos et al. (2020) simulations at $z \sim 7$ (light blue and grey line, respectively) present a 1 dex difference in the lower luminosity with our result in between them. The yellow line and dots indicate the IRLF at $z \sim 5.25$ predicted by the serendipitous galaxies found in the ALPINE survey presented in Gruppioni et al. (2020), whereas the orange symbols show Wang et al. (2019a) results at similar redshift.

3.2 The infrared luminosity function at $z \sim 7$

3.2.1 The stepwise IRLF

In this section, we first present the stepwise LF by using the methodology described in the previous section, before we derive parametric Schechter function fits. Fig. 3 shows the resulting LFs in three equidistant luminosity bins $\log(L_{\text{IR}}/L_{\odot})$: [11.3–11.6], [11.6–11.9], and [11.9–12.2], both for our detections-only and our full sample. The derived stepwise LFs are in excellent agreement, showing that the detection-only sample is not biased significantly. In the rest of the paper, we use the total sample as a baseline.

For the detection-only sample, we further test the possible impact of uncertainties in the IR luminosity estimates. Specifically, we use a Monte Carlo technique in which we perturb the initial L_{IR} measurements by their statistical (Gaussian) uncertainties 10 000 times

and rederive the IRLF in each case. We then use the median and 16th and 84th percentiles, respectively, as the uncertainties. We do not find significant differences in the resulting LF values, but the uncertainties are increased as can also be seen in Fig. 3.

3.2.2 Schechter function fits

We now derive a parametric estimate of the IRLF based on the classic Schechter function from Schechter (1976), commonly used both in the local and the high- z Universe (Johnston 2011). The three parameters that define the Schechter function are ϕ^* , L_* , and α : the normalization factor of the overall density of galaxies, the characteristic luminosity, and the faint-end luminosity slope, respectively. Because of the lack of data at low L_{IR} , we have restricted α taking into account the faint-end slope values found in the literature (see Section 5 for details). We fix the slope to $\alpha = -1.3$ in our fitting,

Table 1. Summary of the main parameters of this study. The first column shows the faint luminosity slope (α), and the second column shows the luminosity function (LF) at the determined luminosity bin (third column). Finally, the fourth column shows the obscured star formation rate density (SFRD) taking into account the three luminosity bins. The first row shows the best-fitting Schechter function parameters for a fixed slope of $\alpha = -1.3$, while the subsequent rows show the total sample and only with detections.

α	$\log(L^*)$ (L_\odot)	$\log(\phi_{\text{IR}})$ ($\text{dex}^{-1} \text{Mpc}^{-3}$)	$\log(\text{SFRD})$ ($\text{M}_\odot \text{yr}^{-1} \text{Mpc}^{-3}$)
Schechter function fit			
-1.3 (fix)	$11.60^{+0.23}_{-0.13}$	$-4.38^{+0.38}_{-0.35}$	$-2.66^{+0.17}_{-0.14}$
Total sample	11.45	$-4.3^{+0.1}_{-0.1}$	-2.93 ± 0.20
	11.75	$-4.6^{+0.2}_{-0.2}$	
	12.05	$-5.5^{+0.4}_{-0.5}$	
Detections	11.45	$-4.4^{+0.2}_{-0.2}$	-3.21 ± 0.18
	11.75	$-4.6^{+0.3}_{-0.3}$	
	12.05	$-5.1^{+0.2}_{-0.5}$	

which is the value derived for the ALPINE high- z IRLF in Gruppioni et al. (2020).

We use a Bayesian Markov chain Monte Carlo (MCMC) approach to derive the posterior distribution of the Schechter function parameters. Hence, we compute the ϕ_{IR} , L_* , while keeping the slope fixed at $\alpha = -1.3$. We have set these initial parameters centred at the values obtained by minimizing the error function first ($\log(\phi_{\text{IR}}) = -3.5$, $\log(L^*) = 11.7$), and then use non-informative Gaussian priors. We then perform 20 000 MCMC iterations and ensure that these are converged. We find that the posterior distribution of the parameters is similar in both cases, either including the total sample (considering upper limits) or only detections. Therefore, we only present the Schechter function with uncertainties for the total sample in Fig. 3. The 1σ uncertainty of the fit function was also calculated from the MCMC chains computing the 16th and 84th percentiles of the posterior distributions. The ϕ_{IR} uncertainties in the fainter end are ~ 0.5 dex, while at the brighter end they are < 0.2 dex. The IRLF is best constrained in the range $11.5 < \log(L_{\text{IR}}/L_\odot) < 12$, and shows that the density of sources drops quickly ($\log(\phi_{\text{IR}}) < -6.5 \text{ dex}^{-1} \text{Mpc}^{-3}$) at luminosities above $\log(L_{\text{IR}}/L_\odot) > 12.3$.

The resulting Schechter function parameters are $\log(\phi_{\text{IR}}) = -4.38^{+0.38}_{-0.35} \text{ dex}^{-1} \text{Mpc}^{-3}$ and $\log(L_*/L_\odot) = 11.60^{+0.23}_{-0.13}$ with a fixed $\alpha = -1.3$ (see Table 1 for the summary of the main parameters). Our analysis shows a $z \sim 7$ IRLF with a considerable number of LIRGs that drop in the ULIRG range suggesting a limit in luminosity at $\log(L_{\text{IR}}/L_\odot) \sim 12.3$. This is in general agreement with some theoretical studies. The IRLF at $L_{\text{IR}} < 11.5 L_\odot$ is uncertain and a larger study with fainter galaxies should be carried out to accurately measure the IRLF at the fainter luminosity end.

We compared our results to both theoretical and observational IRLF studies at similar redshifts (see dashed and continuous lines, respectively, in Fig. 3). Generally, our results are in broad agreement with some simulated IRLFs at similar redshift. When comparing to lower redshift observations at $z \sim 5-6$, however, we find that our IRLF is more than an order of magnitude lower. Finally, our IRLF shows an interesting evolution with redshift, compared with the literature, not only in number density (as was previously shown in Koprowski et al. 2020; Fujimoto et al. 2023), but also in L_* . This could be due to our UV-selected sample being biased towards bright sources and further study with a similar selection at different redshift should be carried out to confirm the possibility of evolution with L_* .

We discuss the points above in more detail in Section 5. We also discuss in Section 5.3 the importance that our data is UV-bright selected that cannot take into account extremely dust-obscured sources that are faint in the UV.

4 OBSCURED STAR FORMATION RATE DENSITY

In this section, we calculate the obscured star formation rate density (SFRD) directly through the IRLF derived in the previous section. We calculate the SFRD in two different ways: (1) by simply summing up the stepwise IR densities for the data in the REBELS sample and (2) by integrating the Schechter IRLF over the luminosity range $10.5 < \log(L_{\text{IR}}/L_\odot) < 13$. These limits were selected in the range over which we can define the Schechter function. Note that the integration limits are narrow but, due to the luminosity bins, there are no data to constrain a lower limit integration. Further analysis is produced in Section 5. In both cases we use a conversion factor $\kappa = 10^{-10} \text{M}_\odot \text{yr}^{-1} L_\odot^{-1}$.

For the stepwise estimates, we considered both the total sample and detections. We find $\log(\text{SFRD}/(\text{M}_\odot \text{yr}^{-1} \text{Mpc}^{-3})) = -3.21 \pm 0.18$ taking only into account the dust continuum detections, which is slightly lower than for the total sample with $\log(\text{SFRD}/\text{M}_\odot \text{yr}^{-1} \text{Mpc}^{-3}) = -2.93 \pm 0.20$. This SFRD estimate needs to be considered as a lower limit since it only takes into account the three luminosity bins.

To extrapolate to fainter luminosities, we have calculated the SFRD for the Schechter LFs. In particular, we use the MCMC chains to derive the median posterior SFRD and the associated uncertainties. We find $\log(\text{SFRD}/\text{M}_\odot \text{yr}^{-1} \text{Mpc}^{-3}) = -2.66^{+0.17}_{-0.14}$ where the uncertainties correspond to the 16th–84th percentile (see Fig. 4). As expected, this SFRD is larger than the SFRD calculated from the observations, since it is integrated over the full luminosity range ($10.5 < \log(L_{\text{IR}}/L_\odot) < 13$). Notice that REBELS is a UV-selected sample and the obscured SFRD needs to be taken into account as a robust lower limit (see caveats in Section 5.3). Finally, the SFRD was computed by adding the serendipitous sources from the REBELS sample presented in Fudamoto et al. (2021). The sum of the two points, UV-selected galaxies and serendipitous ‘dark’ systems, is $\log(\text{SFRD}/(\text{M}_\odot \text{yr}^{-1} \text{Mpc}^{-3})) = -2.53^{+0.17}_{-0.14}$.

We compare our results with previous studies in the literature for both similar samples to REBELS and other dusty galaxies at high redshift. Our derived obscured SFRD of the REBELS sample is 13 ± 1 per cent of the total cosmic SFRD at $z \sim 7$ from Madau & Dickinson (2014) and 9 per cent of the unobscured SFRD estimate from Bouwens et al. (2022b). This is in agreement with the range of obscured SFRD predictions of Zavala et al. (2021), who use a compilation of several surveys to derive a model of the IRLF evolution. Our resulting obscured SFRD lies in the upper part of their inferred SFRD range being the first result at $z \sim 7$ calculated through [CII] spectroscopic scans. In an accompanying paper, Algera et al. (2023) also derived the SFRD for the REBELS sample using the stellar mass as a proxy to calculate the SFRD through a stacking analysis. While our best estimates are a factor of ~ 2.5 lower, the measurements are consistent within the 1σ uncertainties.

In Fig. 4, we also present the obscured SFRD for several studies showing the lack of consensus at $z > 3$ on the obscured SFRD. Our SFRD result is comparable to DSFGs selected at 2 mm from Casey et al. (2021), who report a decrease in the obscured SFRD over $4 < z < 6$. In contrast to these findings, the SFRD from serendipitous sources found in the ALPINE survey presents a non-evolving SFRD

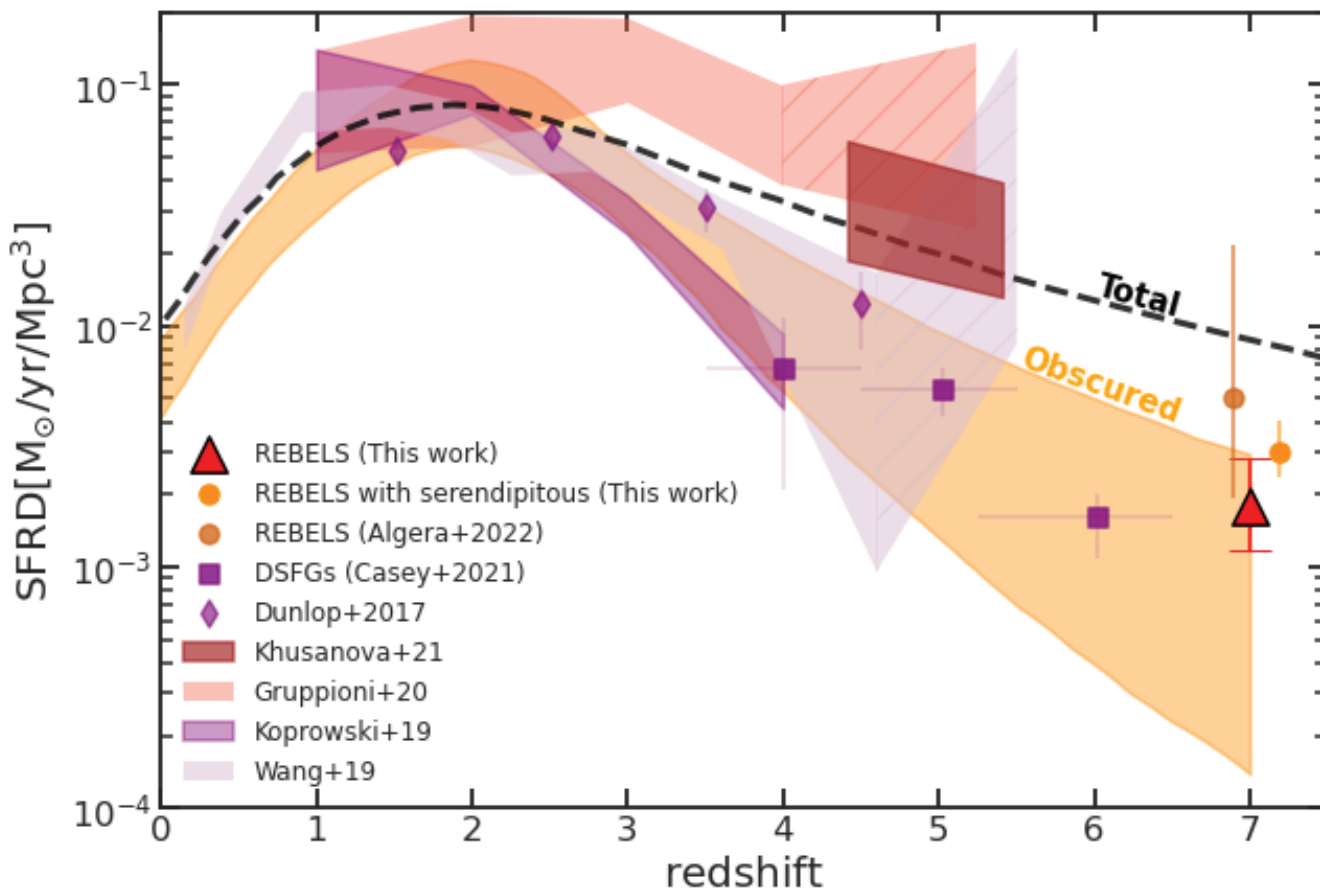


Figure 4. Star formation rate density (SFRD) against redshift for the REBELS sample at $z \sim 7$ and several works in the literature. The black line shows the total SFRD from Madau & Dickinson (2014), whereas the orange shaded region shows the obscured SFRD (Zavala et al. 2021). Our results show a moderate SFRD calculated from the fitted IRLF (red triangle) that increases if the two serendipitous normal dusty REBELS galaxies from Fudamoto et al. (2021) are taken into account (orange dot). Similarly, Algera et al. (2023) obtain a larger contribution to the obscured star formation but in agreement within 1σ error (dark orange dot). DSFGs from the ALMA 2 mm photometric blind survey show a decrease in SFRD over redshift (purple squares; Casey et al. 2021). The 1.3 mm ALMA blind survey presented in Dunlop et al. (2017) shows an obscured SFRD at $1 < z < 4.5$ that decreases at $z > 2$ (purple diamonds). Khusanova et al. (2021) show the SFRD from the ALPINE survey at $z \sim 5$ (brown area). Also from ALPINE, Gruppioni et al. (2020) present a larger obscured SFRD that is decreasing at $z > 3$ (pink area) with the last redshift bin at $z > 4$ containing only one source (dashed pink area). Similarly, Wang et al. (2019a) show a decreasing SFRD (light purple area) with large uncertainty in the last bin at $z \sim 4$ (dashed light purple area). Koprowski et al. (2020) presented a constrained SFRD up to $z \sim 4$ (purple area). REBELS results show the presence of dust at $z \sim 7$ even in UV-selected galaxies.

across the whole redshift range of the sample ($1 < z < 5.5$). Their calculated SFRD is over two orders of magnitude more than our results at $z \sim 7$. Similarly, longer wavelength studies support a flatter evolution of the SFRD at $3 < z < 6$, albeit with more moderate SFRD (Talia et al. 2021). In contrast, our results show lower SFRD at $z \sim 7$, which, when compared to literature at lower redshifts, supports a non-flat SFRD across redshift (see Section 5 for discussion).

5 DISCUSSION

In this section, we compare our IRLF results with observational and theoretical studies. However, due to the underlying assumptions, IRLFs from simulations are not directly comparable. As a result, our findings broadly concur with theoretical research. On the observational side, the literature shows a large range of IRLF suggesting SFRD discrepancies of ~ 2 orders of magnitude. We also explore the causes for the different results in the literature and compare them to our IRLF and SFRD.

5.1 Comparison to literature

Some theoretical IRLFs at $z \sim 6-7$ agree quite well with our findings. For example, Li et al. (in preparation) show a similar IRLF over the luminosity range $10.5 < \log(L_{\text{IR}}/L_{\odot}) < 12.5$, as do the TNG + 300 simulations shown in Shen et al. (2022). But throughout the whole IR luminosity range, the latter exhibits larger number densities by ~ 0.5 dex. A plausible explanation for this shift is the difference in redshift ($\Delta z \sim 1$) between our results and those of Shen et al. (2022), as the IRLF is expected to decrease in number density at increasing redshift (see e.g. Koprowski et al. 2017; Fujimoto et al. 2023).

Our results contrast with those from Lagos et al. (2020) that themselves differ by ~ 0.5 dex despite the fact that both utilize semi-analytical models based on merger trees. Over the full range of our directly observed luminosities ($\log(L_{\text{IR}}/L_{\odot}) > 11.5$), our results are higher than both of these estimates.

Although the simulations described above are based on different assumptions, the theoretical work does not contain a UV-selected sample bias. This suggests that, according to simulations, our

IRLF estimate is not missing a significant number of extremely luminous, UV-undetected galaxies at $z \sim 7$ (for potential caveats, see Section 5.3).

We continue by contrasting with semi-empirical models from Zavala et al. (2021) at $z \sim 7$. Their IRLF changes very little at $12 < \log(L_{\text{IR}}/L_{\odot}) < 12.5$, whereas our IRLF sharply declines. Our study shows an IRLF an order of magnitude higher for LIRGs and a negligible number of galaxies with $\log(L_{\text{IR}}/L_{\odot}) > 12.3$. Thus, we find a different distribution also for the bright luminosity end. These differences in IRLF could be explained by the different methodology, due to the lack of observational data at $z \sim 7$, which leads to an extrapolation of their IRLF at higher redshifts. To do that, it is necessary to assume two different slopes for the LIRGs and the ULIRGs that might lead to different outcomes between our study and Zavala et al. (2021).

Finally, we compare our results with IRLFs derived from observations. In particular, we contrast with the ALPINE IRLF, since it is an analogous survey to REBELS, but at lower redshift (see Section 2 for details). Using the ALPINE data, Gruppioni et al. (2020) provide the IRLF at $z \sim 5$ for serendipitous galaxies. Their IRLF agrees with ours for the lower luminosity bin, but the overall normalization is significantly higher. The reason for the difference is the IRLF rely on several factors. First, the redshift difference ($\Delta z \sim 2$) is an obvious reason for the density to be lower. Furthermore, the REBELS sample was UV selected, implying a selection effect that is non-existent in a blind survey (see Section 5.3 for caveats). Another cause for the disparity with Gruppioni et al. (2020) might be the difference in redshift. Their redshifts were calculated with multiband photometry and with only three galaxies at $z \sim 5$. Finally, the differing dust temperature assumptions and the SED fitting may lead to different IR luminosities, but further analysis is required to ensure that the differences are significant.

In order to continue the observational comparison, we contrast the IRLF calculated with the maximum redshift observed to yet in Wang et al. (2019a). This analysis presents an IRLF with bright IR galaxies selected with *Herschel Space Observatory* (Pilbratt et al. 2010) at $z = 5.5$. At the same redshift, their results have a 2 dex greater LF than ours at the bright end, but a smaller overall LF than the one stated in Gruppioni et al. (2020). Again, the expected difference is caused by the disparity in redshift, as does the bias to select massive galaxies with *Herschel*.

5.2 What IRLF is needed to reproduce extreme SFRD?

This section discusses how changes in the IRLF impact the SFRD. Since there is a lack of consensus about obscured SFRDs at $z > 5$, we evaluate the key variables that influence the SFRD computation: the IRLF faint-end slope, the L_{IR} integration limits, and the conversion factor between L_{IR} and SFRD. To do that, we compute the SFRD derived for extreme α and integration limits to determine whether the most extreme SFRD described in the literature could be reproduced. We also discuss the likely causes of these variances.

First, we investigate changes in the IRLF slope. Lower redshift studies frequently find a slope of $\alpha = -1.3$, including more galaxies with lower IR luminosities (Hammer et al. 2012), but some high-redshift studies report shallower faint-end slopes of $\alpha = -0.4$ (Zavala et al. 2021). In Fig. 5, we compute the IRLF for these two extreme cases by using $\alpha = -2$ and -0.4 , respectively. Additionally, we used a wider luminosity range for the integration than in previous sections of this work, allowing for $8 < \log(L_{\text{IR}}/L_{\odot}) < 13$ as in Gruppioni et al. (2020). Nevertheless, we cannot recreate values

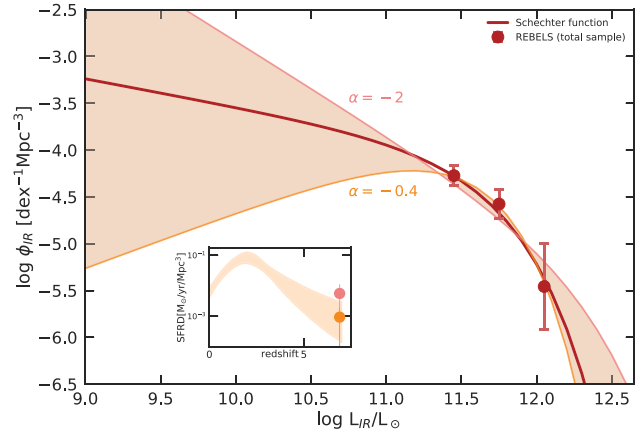


Figure 5. The SFRD depends on the IRLF shape and the luminosity range used in the integration. The faint-end slope α assumed in the low-luminosity end is key for the resulting SFRD. This plot shows the best-fitting IRLF for two extreme slopes: $\alpha = -2$ (red line) and $\alpha = -0.4$ (orange line). The difference between slopes increases in IRLF being ~ 4 orders of magnitude higher at $L_{\text{IR}} = 10^9 L_{\odot}$. The inner plot shows the SFRD for these two extreme cases that shows an order of magnitude difference depending on the slope assumed with the same integration luminosity ($10^8 < L_{\text{IR}}/L_{\odot} < 10^{13}$). The dark red dots show the total REBELS sample for the three luminosity bins. The dark red line shows the Schechter fit with $\alpha = -1.3$ (dark red line) as presented previously in Section 3.

close to their SFRD, even in the most extreme scenario ($\alpha = -2$), yielding a SFRD $\sim 6 \times 10^{-3} M_{\odot} \text{ yr}^{-1} \text{ Mpc}^{-3}$.

This SFRD is, however, consistent with the findings of Talia et al. (2021) (SFRD $\sim 5 \times 10^{-3} M_{\odot} \text{ yr}^{-1} \text{ Mpc}^{-3}$ at $z \sim 5$). It should be noted that the analysis of Talia et al. (2021) was conducted using radio galaxies with median $L_{\text{IR}} = 2.3 \pm 0.5 \times 10^{12} L_{\odot}$, and is thus based on a different set of assumptions than our IR-based estimates.

Despite the fact that it is common to compute the obscured SFRD using the IRLF, some studies directly calculate it by using the individual SFRs. For instance, the Mapping Obscuration to Reionization with ALMA (MORA) survey performed blind 2 mm ALMA observations (Casey et al. 2021), and identified a number of $z \sim 4$ –6 DSFGs. They find SFRD $\sim 10^{-3} M_{\odot} \text{ yr}^{-1} \text{ Mpc}^{-3}$ at $z \sim 6$, which is far lower than the previously mentioned studies such as Talia et al. (2021) or Gruppioni et al. (2020). The key distinction is that their photometric redshift estimates are based on submillimetre data, which can be degenerated with dust temperature. Generally, however, the findings of Casey et al. (2021) are in good agreement with ours, and their obscured SFRD is compatible with a $z \sim 6$ extension of our SFRD at $z \sim 7$. This agreement also extends to the 1.3 mm ALMA serendipitous sources at $z < 4.5$ from Dunlop et al. (2017). Both Dunlop et al. (2017) and Casey et al. (2021) present a decrease of obscured SFRD at $z > 3$ that likely continues beyond $z > 6$, as suggested by our data.

Even if several obscured SFRD present large values at $z \sim 5$ (i.e. Wang et al. 2019a; Gruppioni et al. 2020; Khusanova et al. 2021), we also notice that the highest redshift bin in both Wang et al. (2019a) and Gruppioni et al. (2020) have larger uncertainty than the rest to the low number of sources (as shown the hatched areas in Fig. 4). Given these larger uncertainties, a declining SFRD cannot be excluded from these analyses. Hence, although not in agreement, our results are not in contradiction with the studies that show large SFRDs and the highest redshift surveys. Studies including larger samples at $4 < z < 7$ would be needed to corroborate this hypothesis.

5.3 Possible caveats

In this section, we assess the importance of our data being based on a UV-bright target selection. This directly implies that our study cannot account for extremely dust-obscured sources, such as submillimetre galaxies (SMGs), that are faint in the UV. However, given that there are several verified SMGs at $z > 4$, we know that such galaxies are 100 times less common than UV-based Lyman-break galaxies, given the SMG sky surface density of 0.01 arcmin^{-2} (e.g. Riechers et al. 2013, 2017; Marrone et al. 2018). Furthermore, extremely dusty high-redshift galaxies have only been discovered up to a maximum $z = 6.34$ (Riechers et al. 2013). All of these findings are based on large surveys conducted with the South Pole Telescope (SPT), Submillimetre Common-User Bolometer Array 2 (SCUBA-2), or *Herschel Space Observatory*.

The serendipitous detection of two dust-obscured galaxies in the REBELS data set with similar masses and SFRs as the main sample clearly shows that the primary target sample of REBELS is not complete (Fudamoto et al. 2021). While, the contribution of this class of galaxies to the SFRD is still very uncertain, Fudamoto et al. (2021) estimate a value of $1.2 \times 10^{-3} M_{\odot} \text{ yr}^{-1} \text{ Mpc}^{-3}$, i.e. comparable to our estimate from the IRLF. This would suggest that UV-undetected galaxies could contribute a similar, but additional amount of obscured SFR as UV-bright galaxies.

Similar conclusions have been reached from recent *JWST* observations. The first deep Near-Infrared Camera (NIRCam) observations revealed the existence of UV-undetected, dusty galaxies at $z > 6$. Barrufet et al. (2023), in particular, present the SFRD for high- z dusty galaxies, finding a $\log(\text{SFRD}/M_{\odot} \text{ yr}^{-1} \text{ Mpc}^{-3}) \sim -3$ at $z \sim 7$ for highly attenuated galaxies. We thus conclude that the galaxies we are missing in UV selections might contribute the same order of magnitude as the REBELS sample itself.

To compute a more complete IRLF it would be necessary to perform a deep but blind survey to probe galaxies at $z \sim 7$ at several wavelengths. For the present, a good first step is to obtain results based on the UV-selected REBELS galaxies. These results represent a firm lower limit on the total obscured SFRD at $z \sim 7$.

6 SUMMARY AND CONCLUSIONS

In this work, we have exploited the data from the REBELS survey, which consists of ALMA spectroscopic data of UV-bright galaxies in the EoR. Our sample consists of 42 galaxies at $6.4 < z < 7.7$. 16 have revealed significant dust continuum emission at rest frame $\sim 158 \mu\text{m}$, and all but one of these are spectroscopically confirmed through their [C II] emission lines. This sample was used for the following.

(i) We have calculated the IRLF at $z \sim 7$ for the first time using a spectroscopically confirmed sample. We find a $\log(\phi_{\text{IR}}) \sim -4.2 \pm 0.2 \text{ dex}^{-1} \text{ Mpc}^{-3}$ in our faintest luminosity bin of $\log(L_{\text{IR}}/L_{\odot}) \sim 11.5$. At higher luminosities, the IRLF decreases considerably.

(ii) We have fit a Schechter (1976) function with a fix slope of $\alpha = -1.3$ for the low-luminosity end finding the best-fitting values $\log(\phi_{\text{IR}}) \sim -4.38 \text{ dex}^{-1} \text{ Mpc}^{-3}$ and $\log(L_{\text{IR}}/L_{\odot}) = 11.6$. Our results indicate that extremely luminous galaxies with $\log(L_{\text{IR}}/L_{\odot}) > 12.3$ are extremely rare at $z \sim 7$, with number densities $\log(\phi_{\text{IR}}) < -6.5 \text{ dex}^{-1} \text{ Mpc}^{-3}$.

(iii) We have derived the obscured SFRD through the IRLF. From the observations we calculate a lower limit of $\log(\text{SFRD}/M_{\odot} \text{ yr}^{-1} \text{ Mpc}^{-3}) = -2.93 \pm 0.20$ at $z \sim 7$ that represents ~ 13 per cent of the total SFRD. When integrating over the luminosity range $10.5 < \log(L_{\text{IR}}/L_{\odot}) < 13$ we infer a larger value of $\log(\text{SFRD}/M_{\odot} \text{ yr}^{-1} \text{ Mpc}^{-3}) = -2.66^{+0.17}_{-0.14}$.

(iv) Our IRLF is broadly consistent with some simulations at $z \sim 7$. The inferred SFRD is a robust lower limit that shows a significant contribution of obscured star formation at $z \sim 7$.

We conclude that our results imply a significant amount of obscured SFR at $z \sim 7$ of at least $\log(\text{SFRD}/M_{\odot} \text{ yr}^{-1} \text{ Mpc}^{-3}) \sim -3$. Compared with ALMA blind surveys, our results suggest a steep evolution of the obscured SFRD over redshift that continues to $z \sim 7$, at least.

ACKNOWLEDGEMENTS

We acknowledge the constructive feedback of the referee, Matthieu Bethermin, for his constructive feedback that helped in the improvement of this paper. We acknowledge support from: the Swiss National Science Foundation through the SNSF Professorship grant 190079 (LB and PAO). The Cosmic Dawn Center (DAWN) is funded by the Danish National Research Foundation under grant no. 140. PD acknowledges support from the European Research Council's starting grant ERC StG-717001 ('DELPHI'), from the NWO grant 016.VIDI.189.162 ('ODIN'), and the European Commission's and University of Groningen's CO-FUND Rosalind Franklin program. AF and AP acknowledge support from the ERC Advanced Grant INTERSTELLAR H2020/740120. Generous support from the Carl Friedrich von Siemens-Forschungspreis der Alexander von Humboldt-Stiftung Research Award is kindly acknowledged. YF acknowledges support from NAOJ ALMA Scientific Research grant number 2020–16B. VG gratefully acknowledges support by the ANID BASAL projects ACE210002 and FB210003.

DATA AVAILABILITY

The data used here are available from the REBELS collaboration in the cited papers. Further data products are available from the authors upon reasonable request. All the Figures of the paper can be reproduced with the catalogue in Inami+22 which is public.

REFERENCES

- Adams N. J. et al., 2023, *MNRAS*, 518, 4755
 Algera H. S. B. et al., 2023, *MNRAS*, 518, 6142
 Atek H. et al., 2023, *MNRAS*, 519, 1201
 Barrufet L. et al., 2020, *A&A*, 641, A129
 Barrufet L. et al., 2023, *MNRAS*, 522, 449
 Béthermin M. et al., 2020, *A&A*, 643, A2
 Bouwens R. J. et al., 2015, *ApJ*, 803, 34
 Bouwens R. J. et al., 2021, *AJ*, 162, 47
 Bouwens R. J. et al., 2022a, *ApJ*, 931, 160
 Bouwens R. J., Illingworth G. D., Ellis R. S., Oesch P. A., Stefanon M., 2022b, *ApJ*, 940, 55
 Bouwens R. J., Illingworth G. D., Franx M., Ford H., 2007, *ApJ*, 670, 928
 Bouwens R., 2016, in Mesinger A., ed., *Astrophysics and Space Science Library* Vol. 423, *Understanding the Epoch of Cosmic Reionization*. Springer, Cham, p. 111
 Bowler R. A. A., Bourne N., Dunlop J. S., McLure R. J., McLeod D. J., 2018, *MNRAS*, 481, 1631
 Bowler R. A. A., Jarvis M. J., Dunlop J. S., McLure R. J., McLeod D. J., Adams N. J., Milvang-Jensen B., McCracken H. J., 2020, *MNRAS*, 493, 2059
 Capak P. L. et al., 2015, *Nature*, 522, 455
 Casey C. et al., 2019, *BAAS*, 51, 212
 Casey C. M. et al., 2021, *ApJ*, 923, 215
 Dayal P. et al., 2022, *MNRAS*, 512, 989
 Dayal P., Ferrara A., 2018, *Phys. Rep.*, 780, 1

- Donnan C. T. et al., 2023, *MNRAS*, 518, 6011
- Dunlop J. S. et al., 2017, *MNRAS*, 466, 861
- Dunlop J. S., 2013, in Wiklind T., Mobasher B., Bromm V., eds, *Astrophysics and Space Science Library Vol. 396, The First Galaxies*. Springer-Verlag, Berlin, p. 223
- Endsley R. et al., 2022, *MNRAS*, 517, 5642
- Faisst A. L. et al., 2020, *ApJS*, 247, 61
- Ferrara A. et al., 2022, *MNRAS*, 512, 58
- Finkelstein S. L. et al., 2022, *ApJ*, 940, L55
- Fudamoto Y. et al., 2021, *Nature*, 597, 489
- Fujimoto S. et al., 2023, preprint (arXiv:2303.01658)
- Grupponi C. et al., 2013, *MNRAS*, 432, 23
- Grupponi C. et al., 2020, *A&A*, 643, A8
- Hammer D. M., Hornschemeier A. E., Salim S., Smith R., Jenkins L., Mobasher B., Miller N., Ferguson H., 2012, *ApJ*, 745, 177
- Harikane Y. et al., 2022, *ApJ*, 929, 1
- Harikane Y. et al., 2023, *ApJS*, 265, 5
- Heintz K. E. et al., 2022, *ApJ*, 934, L27
- Hodge J. A., da Cunha E., 2020, *R. Soc. Open Sci.*, 7, 200556
- Hygate A. P. S. et al., 2022, preprint (arXiv:2304.09206)
- Inami H. et al., 2022, *MNRAS*, 515, 3126
- Johnston R., 2011, *A&AR*, 19, 41
- Khusanova Y. et al., 2021, *A&A*, 649, A152
- Koprowski M. P. et al., 2020, *MNRAS*, 492, 4927
- Koprowski M. P., Dunlop J. S., Michałowski M. J., Coppin K. E. K., Geach J. E., McLure R. J., Scott D., van der Werf P. P., 2017, *MNRAS*, 471, 4155
- Labbe I. et al., 2023, *Nature*, 616, 266
- Lagos C. d. P., da Cunha E., Robotham A. S. G., Obreschkow D., Valentino F., Fujimoto S., Magdis G. E., Tobar R., 2020, *MNRAS*, 499, 1948
- Laporte N. et al., 2019, *MNRAS*, 487, L81
- Laporte N., Meyer R. A., Ellis R. S., Robertson B. E., Chisholm J., Roberts-Borsani G. W., 2021, *MNRAS*, 505, 3336
- Le Fèvre O. et al., 2020, *A&A*, 643, A1
- Lim C.-F. et al., 2020, *ApJ*, 889, 80
- Madau P., Dickinson M., 2014, *ARA&A*, 52, 415
- Marrone D. P. et al., 2018, *Nature*, 553, 51
- Naidu R. P. et al., 2022a, *ApJ*, 940, L14, 11
- Naidu R. P. et al., 2022b, *ApJ*, 940, L14
- Nelson E. J. et al., 2022, preprint (arXiv:2208.01630)
- Oesch P. A. et al., 2016, *ApJ*, 819, 129
- Oesch P. A. et al., 2018a, *ApJS*, 237, 12
- Oesch P. A., Bouwens R. J., Illingworth G. D., Labbé I., Stefanon M., 2018b, *ApJ*, 855, 105
- Pilbratt G. L. et al., 2010, *A&A*, 518, L1
- Popping G. et al., 2020, *ApJ*, 891, 135
- Pozzi F. et al., 2021, *A&A*, 653, A84
- Riechers D. A. et al., 2013, *Nature*, 496, 329
- Riechers D. A. et al., 2017, *ApJ*, 850, 1
- Rodighiero G., Bisigello L., Iani E., Marasco A., Grazian A., Sinigaglia F., Cassata P., Grupponi C., 2023, *MNRAS*, 518, L19
- Schaerer D., Marques-Chaves R., Barrufet L., Oesch P., Izotov Y. I., Naidu R., Guseva N. G., Brammer G., 2022, *A&A*, 655, L4
- Schechter P., 1976, *ApJ*, 203, 297
- Schmidt M., 1968, *ApJ*, 151, 393
- Schouws S. et al., 2022a, *ApJ*, 928, 31
- Schouws S. et al., 2022b, preprint (arXiv:2202.04080)
- Shen X., Vogelsberger M., Nelson D., Tacchella S., Hernquist L., Springel V., Marinacci F., Torrey P., 2022, *MNRAS*, 510, 5560
- Smit R. et al., 2018, *Nature*, 553, 178
- Sommovigo L. et al., 2022a, *MNRAS*, 513, 3122
- Sommovigo L. et al., 2022b, *MNRAS*, 517, 5930–5941
- Sommovigo L., Ferrara A., Carniani S., Zanella A., Pallottini A., Gallerani S., Vallini L., 2021, *MNRAS*, 503, 4878
- Stark D. P., 2016, *ARA&A*, 54, 761
- Talia M., Cimatti A., Giulietti M., Zamorani G., Bethermin M., Faisst A., Le Fèvre O., Smolčić V., 2021, *ApJ*, 909, 23
- Topping M. W. et al., 2022, *MNRAS*, 516, 975
- Viero M. P., Sun G., Chung D. T., Moncelsi L., Condon S. S., 2022, *MNRAS*, 516, L30
- Wang L., Pearson W. J., Cowley W., Trayford J. W., Béthermin M., Grupponi C., Hurley P., Michałowski M. J., 2019b, *A&A*, 624, A98
- Wang T. et al., 2019a, *Nature*, 572, 211
- Watson D., Christensen L., Knudsen K. K., Richard J., Gallazzi A., Michałowski M. J., 2015, *Nature*, 519, 327
- Yan L. et al., 2020, *ApJ*, 905, 147
- Zavala J. A. et al., 2021, *ApJ*, 909, 165
- ¹Department of Astronomy, University of Geneva, Chemin Pegasi 51, CH-1290 Versoix, Switzerland
- ²Cosmic Dawn Center (DAWN), Niels Bohr Institute, University of Copenhagen, Jagtvej 128, DK-2200 København N, Denmark
- ³Leiden Observatory, Leiden University, PO Box 9500, NL-2300 RA Leiden, the Netherlands
- ⁴Hiroshima Astrophysical Science Center, Hiroshima University, 1-3-1 Kagamiyama-Higashi, Hiroshima 739-8526, Japan
- ⁵Scuola Normale Superiore, Piazza dei Cavalieri 7, I-56126 Pisa, Italy
- ⁶National Astronomical Observatory of Japan, 2-21-1 Osawa, Mitaka, 169-8555, Tokyo, Japan
- ⁷International Centre for Radio Astronomy Research, University of Western Australia, Stirling Hwy, Crawley 26, WA 6009, Australia
- ⁸Núcleo de Astronomía Facultad de Ingeniería y Ciencias, Universidad Diego Portales, Av Ejército 441, Santiago, Chile
- ⁹Kapteyn Astronomical Institute, University of Groningen, PO Box 800, NL-9700 AV Groningen, the Netherlands
- ¹⁰Waseda Research Institute for Science and Engineering, Faculty of Science and Engineering, Waseda University, 3-4-1 Okubo, Shinjuku, Tokyo 169-8555, Japan
- ¹¹Departamento de Astronomía, Universidad de Chile, Casilla 36-D, Santiago 7591245, Chile
- ¹²Centro de Astrofísica y Tecnologías Afines (CATA), Camino del Observatorio 1515, Las Condes, Santiago 7591245, Chile
- ¹³Dipartimento di Fisica, Sapienza, Università di Roma, Piazzale Aldo Moro 5, I-00185 Roma, Italy
- ¹⁴INAF/Osservatorio Astronomico di Roma, via Frascati 33, I-00078 Monte Porzio Catone, Roma, Italy
- ¹⁵Sterrenkundig Observatorium, Ghent University, Krijgslaan 281-59, B-9000 Gent, Belgium
- ¹⁶Department of Physics and Astronomy, University College London, Gower Street, London WC1E 6BT, UK
- ¹⁷Centre for Astrophysics and Supercomputing, Swinburne University of Technology, PO Box 218, Hawthorn, VIC 3112, Australia
- ¹⁸Departament d'Astronomia i Astrofísica, Universitat de València, C. Dr Moliner 50, E-46100 Burjassot, Valencia, Spain
- ¹⁹Unidad Asociada CSIC 'Grupo de Astrofísica Extragaláctica y Cosmología' (Instituto de Física de Cantabria – Universitat de València), 46980, Valencia, Spain
- ²⁰Steward Observatory, University of Arizona, 933 N Cherry Ave, Tucson, AZ 85721, USA

This paper has been typeset from a \LaTeX file prepared by the author.